Surface Plasmon Polaritons Emission with Nanopatch Antennas: Enhancement by Means of Mode Hybridization

Cheng Zhang, Jean-Paul Hugonin, Jean-Jacques Greffet, Christophe Sauvan

Surface plasmon polaritons emission with nanopatch antennas: enhancement by means of mode hybridization

Cheng Zhang, Jean-Paul Hugonin, Jean-Jacques Greffet and Christophe Sauvan*

Laboratoire Charles Fabry, Institut d'Optique Graduate School, CNRS, Université Paris-Saclay, 91127 Palaiseau, France

Corresponding author: christophe.sauvan@institutoptique.fr

Abstract

We theoretically study the emission of surface plasmon polaritons (SPPs) in cylindrical nanopatch antennas with sub-10-nm dielectric gaps. The eigenmodes of a nanopatch antenna can be classified as gap modes or antenna modes. We show that these two families of modes possess very different intrinsic properties regarding the emission of SPPs. Gap modes have an extremely large Purcell factor, which allows overcoming quenching, but a weak efficiency to radiate SPPs. On the other hand, antenna modes have a weaker Purcell factor but a larger efficiency to radiate SPPs. The coupling between gap modes and antenna modes results in the formation of hybrid modes. We evidence that these hybrid modes have the advantage to provide both a large Purcell factor and a large SPP efficiency. Working with such hybrid modes allows enhancing the SPP emission. We show that the mode hybridization results in an enhancement of two orders of magnitude of the power radiated into propagating SPPs at $\lambda = 800$ nm and an overall SPP efficiency of 15% for a gap thickness of 1 nm. Moreover, increasing the refractive index of the host medium surrounding the nanopatch further improves the SPP emission.

Keywords: nanopatch antenna, dielectric nanogap, surface plasmon emission, quasinormal modes

Spontaneous emission of light is largely affected by the electromagnetic environment.[1,2] It is well-known that the emission rate is proportional to the photonic local density of states (LDOS).[3,4] In the widely-studied case of an emitter coupled to a resonant system, the emission enhancement is given by the Purcell factor, which is proportional to the Q/V ratio, with Q the quality factor of the resonance and V the mode volume.[1] Since the seminal work of Purcell, the progress in micro- and nanofabrication has resulted in experimental demonstrations of spontaneous emission in micro- and nanoresonators with ever smaller volumes.[5-9]

Nowadays, metal-insulator-metal (MIM) nanogaps offer an unprecedented potential to confine a single optical mode into deep-subwavelength volumes. This unique ability has propelled their use in a variety of applications.[10-17] Among them, the realization of nanosources is a very active research topic. Different types of light emitters have been inserted in dielectric nanogaps between metals: fluorescent molecules,[18,19] III-V semiconductor nanorods,[20] and colloidal quantum dots.[21-23] To benefit from the full potential of MIM devices to boost light-matter interactions, the gap thickness has to be smaller than 10 nm, which requires the use of state-of-the-art nanolithography, self-assembly, or molecular linkers. Emission accelerations by three orders of magnitude and radiative efficiencies larger than 40% have been demonstrated with gaps in the range 5-15 nm[18,19] and the strong coupling regime with a single emitter is within reach with gaps of 1 or 2 nm.[8,9] With such extremely small dielectrics gaps between metals, light can also be emitted by inelastic electron tunneling.[24] The efficiency of this light-emission process is fairly poor in planar systems but it can be increased by using a nanoantenna.[25] Recent experimental works used inelastic electron tunneling through nanometer-sized dielectric gaps to demonstrate electrically driven nanosources of light[26-28] and electronic-plasmonic transducers.[29]

In such ultimate regime where the emitter lies at sub-5-nm distances from a metal surface, quenching through nonradiative energy transfer to the metal constitutes a significant limitation that needs to be carefully addressed. Even if plasmonic nanoantennas based on a MIM nanogap have a clear potential to overcome

quenching,[18,19,30,31,32] the system must be engineered with care following specific design rules.[25]

Photon emission from MIM nanogaps has been widely studied.[18-23,26-28,30-32] In this work, we focus on a different process. We present a theoretical study of surface plasmon polaritons (SPPs) emission from MIM nanopatch antennas with sub-10-nm gaps. Nanopatch antennas support different types of modes, which can couple and hybridize for some specific geometries.[33-36] We show that the hybridization of two different modes sustained by a cylindrical nanopatch largely increases both the SPP emission and the SPP efficiency (fraction of the total emission that is funneled into propagating SPPs). We use a rigorous modal formalism to investigate the physical mechanism responsible for this phenomenon. The SPP emission is enhanced when one mode with a large Purcell factor but a poor ability to radiate SPPs is coupled to another mode with a lower Purcell factor but a better ability to radiate SPPs. The hybrid modes resulting from the coupling have the advantage to provide both a large Purcell factor and a good ability to radiate SPPs. The hybridization effect takes place whatever the thickness of the dielectric gap, but it plays a more significant role for small gaps. The optimal geometry at a working wavelength of 800 nm (nanocylinder diameter 39 nm and height 72 nm, dielectric gap thickness of 1 nm) provides i) over two orders of magnitude enhancement for the SPP emission and ii) a SPP efficiency of 15%. The plasmonic efficiency can still be improved by increasing the refractive index of the medium surrounding the metallic nanocylinder.

This article is organized as follows. First, we describe the system under study and the theoretical formalism used for the calculation of SPP emission. We evidence the existence of optimum geometries that maximize the power emitted into SPPs. Then, we develop a modal formalism to interpret the enhancement of SPP emission. In contrast to previous works that have used a modal description of light scattering by nanopatch antennas,[35] we fully take into account the non-Hermitian character of the system by using quasinormal modes.[37-40] Only then can we properly separate the contributions from each mode that add in amplitude and interfere.[37] We derive a closed-form expression of the SPP efficiency as a function of the Purcell factors and the β-factors

of each mode. Our expression also highlights the presence of an interference mechanism between the modes. Thirdly, we study the impact of different geometrical parameters on the mode hybridization and the SPP emission. In the last section, we study the ratio between SPP emission and photon emission, and we show that the refractive index of the medium surrounding the nanopatch has a strong impact on the SPP efficiency.

Surface plasmon polaritons emission

We consider a cylindrical nanopatch antenna as illustrated in Fig. 1(a). The structure is composed of a gold nanocylinder on top of a thin dielectric spacer layer (refractive index $n_d = 1.45$ and thickness H_d) and a gold layer (thickness $H_m = 50$ nm) over a glass substrate (refractive index $n_s = 1.5$). The diameter and height of the gold nanorod are denoted by D and H, respectively. The dielectric permittivity of gold is given by a Drude-Lorentz model that fits the data tabulated in Ref. 41 over the [500-1500] nm spectral range (see Supporting Information).

A vertically polarized electric dipole is buried in the middle of the dielectric layer at half distance from both metal surfaces and on the cylinder axis. An electric dipole is the usual classical model for light emission by a two-level system. It is also used to model light emission by inelastic electron tunneling.[25,28,42] We compute the emission of the dipole source with an aperiodic Fourier modal method dedicated to body-of-revolution structures.[43] From the calculation of the electromagnetic field, we extract four important physical quantities:

(i) the total power emitted by the source P_T,

(ii) the radiative power P_r (power radiated into the far-field),

(iii) the non-radiative power P_{nr} (power dissipated in the metal),

(iv) the amplitude A_{spp} of the SPP that propagates away from the cylinder.

The total power is proportional to the imaginary part of the total electric field at the source position projected along the source polarization.[4] The radiative power P_r is the sum of the powers radiated in air and in the dielectric substrate. The radiative power P_r

and the SPP amplitude A_{spp} are calculated from the near field thanks to a near-to-far field transformation valid both for plane waves and guided modes.[25,44] Because of the emission of SPPs, light is absorbed along the metal film up to distances from the antenna that are larger than the wavelength. Therefore, a direct calculation of the absorption would require a computation of the electric field far from the antenna over a large calculation domain. It is more accurate to deduce the non-radiative power from energy conservation, $P_{nr} = P_T - P_r$.

We briefly recall the main steps of the calculation of the SPP amplitude. The interested reader can find more details in Refs. 25 and 44. Outside the antenna, the electric field emitted by a point source located on the cylinder axis and polarized vertically can be expanded as

$$\mathbf{E}(r,z) = A_{spp}\mathbf{E}^{+}_{spp}(r,z) + \sum_{\sigma} A_{\sigma}\mathbf{E}^{+}_{\sigma}(r,z) \ , \qquad (1)$$

where the last term corresponds to a summation over the continuum of radiation modes of the planar gold/dielectric/air system. The first term is the part of interest; it corresponds to the field of an outgoing SPP with an amplitude A_{spp}. Note that the fields are independent of the azimuthal angle θ because of the source position and polarization. The SPP amplitude is simply given by an overlap integral,[25,44]

$$A_{spp} = \frac{1}{N_{spp}} \iint \left(\mathbf{E}^{-}_{spp} \times \mathbf{H} - \mathbf{E} \times \mathbf{H}^{-}_{spp}\right) \cdot \mathbf{u}_r r d\theta dz = \left\langle \boldsymbol{\phi} \middle| \boldsymbol{\phi}^{-}_{spp} \right\rangle \ , \qquad (2)$$

where $\boldsymbol{\phi} = (\mathbf{E}, \mathbf{H})$ is the total electromagnetic field emitted by the source and $\boldsymbol{\phi}^{-}_{spp} = (\mathbf{E}^{-}_{spp}, \mathbf{H}^{-}_{spp})$ is the field of the ingoing SPP. The latter is normalized such that $N_{spp} = -16/k_{spp}$, with k_{spp} the SPP propagation constant.[44] Since it relies on the orthogonality of the modes supported by the planar system, Eq. (2) is independent of the radial position r provided that the cylindrical surface is chosen outside the antenna.

We define the power emitted into SPPs as (see Supporting Information)

$$P_{spp} = \frac{4}{|k_{spp}|} \left|A_{spp}\right|^2, \qquad (3)$$

and the antenna efficiency to generate SPPs as

$$\eta_{spp} = \frac{P_{spp}}{P_T} \ . \qquad (4)$$

Let us emphasize that, since the gold layer has a finite thickness ($H_m = 50$ nm), the SPP propagating away from the antenna is a leaky wave that radiates energy in the dielectric substrate. Therefore, the power P_{spp} carried out by the SPP contains both a radiative part (leakage into the substrate) and a non-radiative part (absorption along the metal surface as the SPP propagates). It is not straightforward to properly separate the radiative part of P_{spp} from its non-radiative part. Thus, it is important to keep in mind that P_{spp} shall only be used with care in an energy balance.

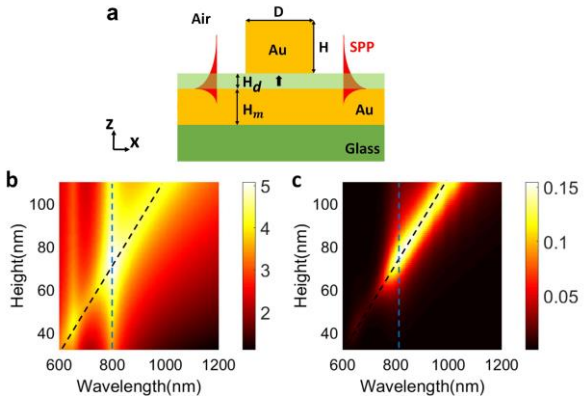

Figure 1. (a) Schematic of the cylindrical nanopatch antenna under study. A gold nanocylinder (diameter D and height H) lies on top of a dielectric (thickness H_d) – gold (thickness H_m =50 nm) – glass stack. The refractive indices of the dielectric spacer and the glass substrate are $n_d = 1.45$ and $n_s = 1.5$, respectively. The vertical arrow marks the position and polarization of the dipole source. (b) SPP power P_{spp}, see Eq. (3), as a function of the wavelength and the nanopatch height. The SPP power is normalized by the power emitted in a bulk material of refractive index n_d and plotted in log scale. (c) SPP efficiency η_{spp}, see Eq. (4), as a function of the wavelength and the height. In (b)-(c), the nanopatch diameter is $D = 39$ nm and the gap thickness is $H_d = 1$ nm. The dashed lines are guides to the eye that follow the two resonances.

We calculate the total emitted power P_T and the power emitted into SPPs P_{spp} as a function of the wavelength and the antenna height H for a fixed diameter $D = 39$ nm. Figure 1(b) shows the SPP power in log scale and Fig. 1(c) displays the SPP efficiency η_{spp}. The SPP power exhibits two clear resonances; one resonance at $\lambda = 800$ nm that does not vary with the antenna height and a second resonance that redshifts significantly as the antenna height is increased. Both resonances cross at

$\lambda = 800$ nm and $H = 72$ nm. At the crossing point, the power emitted into SPPs is enhanced by one order of magnitude compared to other geometries. This enhancement is not due to an overall increase of the power emitted by the source. It corresponds to an increase of the SPP efficiency, as shown in Fig. 1(c).

This result evidences that there exist optimum geometries of the nanopacth antenna that optimize the SPP efficiency. As shown by Fig. 1(b), the optimum arises from the coupling between two different modes of the antenna. To clarify the mechanism of the SPP efficiency enhancement by a mode hybridization, we have developed a modal formalism of the SPP emission. Before presenting the modal formalism, let us first briefly describe the modes of the cylindrical nanopatch that are involved in the coupling of Figs. 1(b)-(c).

Modes of a cylindrical nanopatch

A cylindrical nanopatch antenna supports different eigenmodes. Because of the symmetry of revolution, each mode can be characterized by an azimuthal number m; the electromagnetic field varies as $\exp(im\theta)$, with θ the angle of cylindrical coordinates. The eigenmodes of such a nanoparticle-on-mirror can be sorted in two different families.[33-36] On the one hand, a gold nanorod alone sustains localized plasmonic modes. As the nanorod is brought close to the gold layer, these modes couple to their mirror images. Following Ref. 34, we refer to these modes as longitudinal antenna modes and we denote them with the label L_{mn}, with m the azimuthal number and n the mode order. On the other hand, the thin dielectric gap surrounded by metal acts as a transverse channel that supports so-called gap SPPs.[45-47] Because of reflection at the cylinder edges, the gap SPPs propagate back and forth below the patch and build standing waves when the accumulated phase during one round trip matches 2π. We refer to these Fabry-Perot-like modes as transverse gap modes[34] and we denote them with the label S_{mn}, with m the azimuthal number and n the mode order. The order n corresponds to the number of nodes of the vertical electric-field component E_z below the patch.

The antenna height H is the good parameter to discriminate both families of

modes. Indeed, the eigenfrequency of the antenna modes L_{mn} strongly varies with H whereas the gap modes S_{mn} are almost independent of a variation of H, see Fig. 1(b) On the contrary, the diameter D impacts both L_{mn} and S_{mn} modes. For most geometries, both types of modes can be easily identified since they are well separated in the parameter space. However, for some geometries, the modes from the L and S families couple.[34,35] Mode hybridization in a cylindrical patch is driven by the following selection rule: only modes with the same azimuthal number can couple.

The modes involved in the coupling shown in Fig. 1(b) are the first-order antenna mode L_{01} and the second-order gap mode S_{02}. As illustrated in Fig. 2(a), the L_{01} mode sustains an electric-dipole-like charge distribution. The charge distribution of the S_{02} mode is shown in see Fig. 2(b). Note that most studies of photon emission with nanocubes-on-mirror have used the first-order gap mode S_{11}, which corresponds to an electric-quadrupole-like charge distribution, see Fig. 2(c).[18,23,30,31] Since its azimuthal number is $m = 1$, this mode is not excited by a vertically polarized dipole located on the cylinder axis, which can only excite modes with $m = 0$. Moreover, the S_{11} gap mode cannot couple to the antenna mode L_{01} because of different azimuthal numbers.

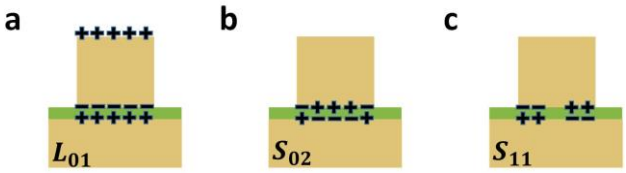

Figure 2. Schematic of the charge distributions corresponding to (a) the first-order antenna mode L_{01}, (b) the second-order gap mode S_{02}, (c) the first-order gap mode S_{11}.

Modal formalism for the SPP emission

Due to energy dissipation by absorption and radiation, a plasmonic nanoresonator is a non-Hermitian system and its eigenmodes are quasinormal modes (QNMs).[37,38] We use the modal formalism developed in Ref. 37 for photon emission and extend it to SPP emission. Calculating the QNMs and their excitation coefficients allows us to define modal physical quantities such as the Purcell factor, the β-factor, or the modal SPP efficiency. Then, we derive a simple closed-form expression of the SPP efficiency of

the antenna as a function of the modal quantities. This closed-form expression provides i) design rules to improve the SPP efficiency and ii) an in-depth interpretation of the SPP efficiency enhancement observed in Fig. 1.

The total electric field $\mathbf{E}$ emitted by the dipole source can be expanded as a sum of QNMs.[37,38] According to Fig. 1(b), the nanopatch sustain two resonances in the spectral range of interest. In the QNM expansion, we separate the modes responsible for the resonances (labelled 1 and 2) from all the others,

$$\mathbf{E}(\mathbf{r},\omega) = \alpha_1(\omega)\mathbf{E}_1(\mathbf{r}) + \alpha_2(\omega)\mathbf{E}_2(\mathbf{r}) + \sum_{p\neq 1,2}\alpha_p(\omega)\mathbf{E}_p(\mathbf{r}) \ . \qquad (5)$$

For an emitting dipole $\mathbf{p}$ located at $\mathbf{r}_0$, the excitation coefficients are given by $\alpha_m(\omega) = -\omega\mathbf{p}\cdot\mathbf{E}_m(\mathbf{r}_0)/(\omega-\tilde{\omega}_m)$. Each mode is characterized by a field profile $\mathbf{E}_m(\mathbf{r})$ and a complex eigenfrequency $\tilde{\omega}_m = \omega_m - i\frac{\omega_m}{2Q_m}$. The real part of $\tilde{\omega}_m$ gives the resonance frequency and the imaginary part is related to energy dissipation through the quality factor Q_m.

Since it is related linearly to the imaginary part of the total field, the total power can also be separated in three contributions,[37,38]

$$P_T(\omega) = P_1(\omega) + P_2(\omega) + P_q(\omega) \ , \qquad (6)$$

where P_m is the power emitted into mode m ($m = 1,2$) and P_q is the power emitted into all the other QNMs. In the case under study, the contribution of higher-order QNMs, whose eigenfrequencies lie outside the spectral range of interest, corresponds mainly to quenching, as shown in Ref. 48 and in Supporting Information (see Fig. S3). Therefore, P_q is mostly a non-radiative power that is dissipated in the metal in a nanoscale volume close to the source.

The power emitted into a mode at resonance defines its Purcell factor,

$$F_m = \frac{P_m(\omega_m)}{P_0} = \frac{3}{4\pi^2}\left(\frac{\lambda_m}{n_d}\right)^3 Q_m \mathrm{Re}\left(\frac{1}{V_m}\right) \ , \qquad (7)$$

where $m = 1,2$, $\lambda_m = 2\pi c/\omega_m$, and P_0 is the power emitted by the same dipole in a bulk material of refractive index n_d. For a QNM, because of energy dissipation, the mode volume V_m is a complex quantity.[37,38] We define also the β-factor, which gives the fraction of the total emission that is funneled into one mode,

$$\beta_m = \frac{P_m}{P_T} = \frac{P_m}{P_1+P_2+P_q} \ , \tag{8}$$

with $m = 1,2$. For a source located at sub-10-nm distances from the metal, quenching is huge and $P_q/P_0 \gg 1$. Therefore, the β-factor is extremely small except if the Purcell factor is large enough to compete with quenching.

Let us now define the modal SPP power and the modal SPP efficiency. Since Eqs. (2) and (5) are linear, the total SPP amplitude is the sum of the SPP amplitudes provided by each mode. The modal SPP amplitude A_{spp}^m, i.e., the fraction of the SPP amplitude that is solely due to mode m, is given by

$$A_{spp}^m = \alpha_m(\omega)\langle \boldsymbol{\phi}_m | \boldsymbol{\phi}_{spp}^- \rangle \ , \tag{9}$$

with the bra-ket notation introduced in Eq. (2) for the overlap integral. From the modal SPP amplitude, we can define the SPP power that is due to mode m as

$$P_{spp}^m = \frac{4}{|k_{spp}|} \left| A_{spp}^m \right|^2 \ , \tag{10}$$

and the modal SPP efficiency as

$$\eta_{spp}^m = \frac{P_{spp}^m}{P_m} \ , \tag{11}$$

with $m = 1,2$. The modal SPP efficiency η_{spp}^m is the good figure of merit to quantify the ability of a given mode to radiate SPPs. Let us see now how the total SPP efficiency of the antenna can be easily deduced from the modal efficiencies.

Since the overlap integral in Eq. (9) is calculated outside the antenna whereas higher-order modes are tightly confined around the antenna, we assume that only modes 1 and 2, which are responsible for the resonances, contribute to SPP emission: $A_{spp}^p \approx 0$ for $p \neq 1,2$. Therefore, the SPP power is given by

$$P_{spp} \approx P_{spp}^1 + P_{spp}^2 + P_{12} \ . \tag{12}$$

with

$$P_{12} = 2\mathrm{Re}\left(A_{spp}^1 {A_{spp}^2}^*\right). \tag{13}$$

The cross power P_{12} results from the interference between the SPP amplitude radiated by mode 1 and the one radiated by mode 2, which are not necessarily in phase. Finally,

the total SPP efficiency of the antenna can be written as

$$\eta_{spp} = \frac{P_{spp}}{P_T} \approx \beta_1 \eta_{spp}^1 + \beta_2 \eta_{spp}^2 + \frac{P_{12}}{P_T} \ . \quad (14)$$

This closed-form expression is a central result of this article. It evidences that the total SPP efficiency of the antenna is directly related to the ability of the excited modes to radiate SPPs (the modal efficiencies η_{spp}^m) provided that these modes have a large β-factor, i.e., their Purcell factor is strong enough to compete with quenching. The physical meaning of the cross term P_{12} is less straightforward. Depending on their field profiles, see Eq. (9) and (13), the modes can interfere constructively or destructively. We will see that this interference mechanism cannot be neglected when both modes are hybridized. Note that most of the nanopatch antennas studied in the literature are working in the single-mode regime. In that case, Eq. (14) reduces to $\eta_{spp} = \beta_1 \eta_{spp}^1$.

Calculation of the nanopatch modes and their characteristics

In order to understand the increase of SPP emission observed in Fig. 1, we have calculated the antenna mode L_{01} and the gap mode S_{02} as well as their Purcell factors, β-factors, and modal SPP efficiencies. Even if it is not excited by a vertically polarized source located on the axis, we have also calculated the first-order gap mode S_{11} for completeness, since it has been widely used in nanocubes-on-mirror.[18,23,30,31] Figure 3 gathers our main results for a fixed diameter of the nanopatch ($D = 39$ nm) and a fixed thickness of the dielectric gap ($H_d = 1$ nm). We have calculated the three modes L_{01}, S_{02}, and S_{11} as a function of the cylinder height H.

Figure 3(a) shows the real part of the eigenfrequencies and the mode linewidths (imaginary part of the eigenfrequencies). Points A, B and C are located far from any coupling ($H = 120$ nm) and mark respectively the gap mode S_{02}, the antenna mode L_{01}, and the gap mode S_{11}. As the cylinder height decreases, the antenna mode L_{01} blueshifts (red curve) while the frequencies of the gap modes S_{02} and S_{11} remain almost unchanged (blue and black curves). Points D and E mark the hybrid modes resulting from the coupling between the gap mode S_{02} and the antenna mode L_{01} for

$H = 72$ nm. We observe an anti-crossing of the eigenfrequencies with a splitting smaller than the mode linewidths. Since the antenna mode L_{01} and the gap mode S_{11} share different azimuthal numbers, their eigenfrequencies simply cross without coupling at $\lambda = 1040$ nm and $H = 120$ nm. Points G and H mark respectively the antenna mode L_{01} and the gap mode S_{02} on the other side of the coupling region for cylinder heights smaller than 72 nm.

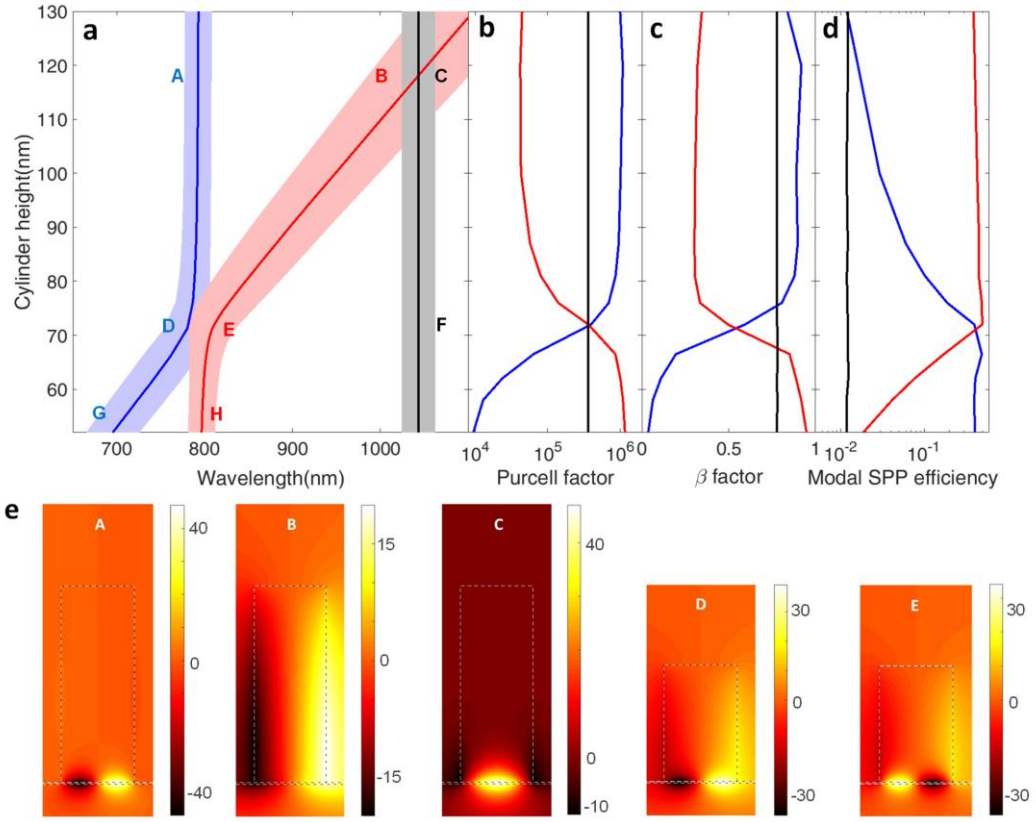

Figure 3. Evolution of the modes of a cylindrical nanopatch with the cylinder height H for $D = 39$ nm and $H_d = 1$ nm. (a) Eigenfrequencies of the three modes under study. The black line C-F shows the S_{11} mode. The blue (A-D-G) and red (B-E-H) lines show the hybrid modes that arise from the coupling between the S_{02} gap mode and the L_{01} antenna mode.. The solid curves give the resonance wavelength and the colored area represent the mode linewidth (quality factor). The coupling between S_{02} and L_{01} modes occurs for $H = 72$ nm. (b) Purcell factors of the three modes in (a) as defined in Eq. (7). (c) β-factors of the three modes in (a) as defined in Eq. (8). (d) Modal SPP efficiencies of the three modes in (a) as defined in Eq. (11). (e) Magnetic-field distributions $\mathrm{Im}(H_y)$ in the (x, z) plane. From left to right: S_{02} gap mode at point A, L_{01} antenna mode at point B, S_{11} gap mode at point C, hybridized modes resulting from the coupling between L_{01} and S_{02} modes at points D and E.

The impact of the hybridization on the field distributions of the different modes is shown in Fig. 3(e). From left to right, we show the magnetic-field distributions $\mathrm{Im}(H_y)$ of the uncoupled gap mode S_{02} at point A, the uncoupled antenna mode L_{01} at point B, the gap mode S_{11} at point C, and both hybrid modes at points D and E. The field of the hybrid modes is clearly a mixture of the fields of the uncoupled L_{01} and S_{02} modes.

The Purcell factors are shown in Fig. 3(b) as a function of the antenna height H. The Purcell factor of the gap mode S_{11} is constant and extremely large, of the order of 4×10^5. Outside the coupling region, the gap mode S_{02} has also a huge Purcell factor of 10^6 whereas the antenna mode L_{01} has a relatively smaller Purcell factor of 4×10^4. The mode hybridization for $H = 72$ nm yields an increase by one order of magnitude of the Purcell factor of the antenna mode L_{01}. Both hybrid modes have a comparable Purcell factor on the order of 4×10^5. As can be seen from the linewidths in Fig. 3(a), the quality factors are only weakly impacted by the coupling. The increase of the Purcell factor mainly results from a decrease of the mode volume (see SI).

Since the quenching P_q only weakly varies over the considered spectral range, the β-factors show the same trend as the Purcell factors, see Fig. 3(c). It is noteworthy that, thanks to its huge Purcell factor, the uncoupled gap mode S_{02} has a β-factor larger than 80%. This mode provides such an extreme light confinement that its excitation overcomes the huge LDOS associated to quenching, which is of the order of 10^5 times the vacuum LDOS (see Supporting Information Fig. S1). The uncoupled antenna mode L_{01} has a smaller β-factor, which is increased when the modes are hybridized.

We now turn to the SPP modal efficiency displayed in Fig. 3(d). The downside of the extreme confinement of the gap modes are their low efficiency to radiate SPPs of the order of 1%. They overcome quenching but do not really improve the overall SPP emission. On the other hand, the antenna mode L_{01}, whose field extends more around the cylinder, radiates SPPs with an efficiency of 40%. The coupling mixes the mode characteristics and both hybrid modes have a good modal SPP efficiency up to 40%.

In summary, the gap modes S_{02} and S_{11} provide an extremely large Purcell factor (larger than 4×10^5) that is able to compete with quenching – most of the emission

is funneled into the mode, $\beta > 80\%$ – but a negligible modal SPP efficiency, $\eta_{spp}^{m} \approx 1\%$. On the other hand, the antenna mode L_{01} has a much better SPP efficiency ($\eta_{spp}^{m} \approx 40\%$) but, due to its smaller Purcell factor, does not fully overcome quenching since $\beta < 40\%$. When these modes with different characteristics are coupled, the resulting hybrid modes retain the best properties of both worlds: a large Purcell factor and a large modal SPP efficiency.

To fully evaluate the SPP efficiency of the antenna with the modal formalism, we need to calculate the cross term P_{12} in Eq. (14), which is due to the interference between the SPPs radiated by both modes. Its spectrum is displayed in Fig. 4. Unfortunately, the SPPs generated by the hybrid modes are not in phase and they interfere partially destructively, $P_{12} < 0$. The sign of the interference term mostly depends on the field profiles of the nanopatch modes, see Eqs. (9) and (14). However, the mode hybridization still results in an increase of the SPP power and the SPP efficiency, as shown in Fig. 1. A comparison between the predictions of the modal formalism with only two modes and the results of a rigorous calculation is shown in Supporting information Fig. S3. The good agreement that we obtain validates the assumption to neglect the contribution of higher-order modes in the SPP generation.

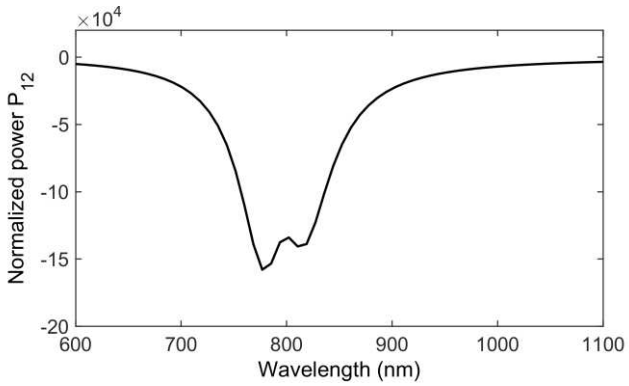

Figure 4. Spectrum of the power P_{12} (normalized by the power emitted in a bulk material of refractive index n_d) that results from the interference of the SPPs emitted by both hybrid modes, see Eqs. (12)-(13). The interference is destructive ($P_{12} < 0$) over the whole spectrum.

Dependence of the mode hybridization on the antenna geometry

Let us now investigate the impact of the nanopatch diameter and the gap thickness on the mode hybridization and the resulting SPP emission enhancement. As the nanopatch geometry is varied, both S_{02} and L_{01} modes shift spectrally but there exists always a height H for which they couple. Thanks to the positive impact of mode hybridization evidenced in the previous section, this height provides the optimal geometry for maximizing the SPP power and the SPP efficiency.

The SPP efficiency spectrum of the optimal geometry is plotted in Fig. 5 for four different values of the diameter, $D = 25$ nm, 40 nm, 56 nm, and 90 nm, that correspond to four different working wavelengths of 615 nm, 710 nm, 790 nm, and 900 nm. Since the gap modes have been the most widely used in nanopatch antennas made of nanocubes-on-mirror, we have chosen as a reference geometry a nanopatch with the same resonance frequency that supports a gap mode S_{02} alone away from the coupling region. The reference geometries have an almost constant aspect ratio $H/D \approx 0.23$. Whatever the nanopatch diameter, the mode hybridization results in an increased SPP efficiency. For $D = 25$ nm, 40 nm, 56 nm, and 90 nm, the SPP efficiency is enhanced by a factor of 170, 290, 180 and 70, respectively. As the nanopatch diameter increases, the resonance redshifts and both the optimal height and the SPP efficiency increase.

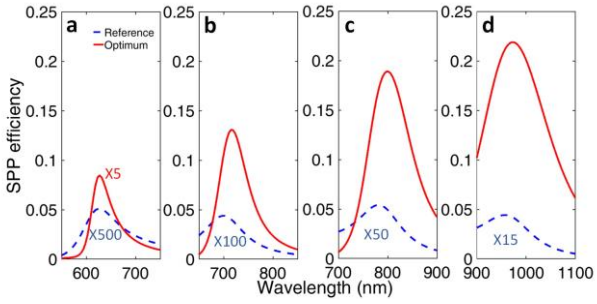

Figure 5. SPP efficiency spectrum for different values of the nanopatch diameter and a fixed gap thickness $H_d = 1.5$ nm. The optimal geometry (red curve) is compared to a reference geometry (blue dashed curve) with the same resonance frequency (S_{02} mode alone away from the coupling region). (a) $D = 25$ nm. The optimal geometry (spectrum multiplied by a factor of 5) and the reference (spectrum

multiplied by a factor of 500) correspond respectively to $H = 29.5$ nm and $H = 6$ nm. (b) $D = 40$ nm. The optimal geometry and the reference (spectrum multiplied by a factor of 100) correspond respectively to $H = 58$ nm and $H = 9$ nm. (c) $D = 56$ nm. The optimal geometry and the reference (spectrum multiplied by a factor of 50) correspond respectively to $H = 82$ nm and $H = 13$ nm. (d) $D = 90$ nm. The optimal geometry and the reference (spectrum multiplied by a factor of 15) correspond respectively to $H = 123$ nm and $H = 22$ nm.

To study the impact of the gap thickness on the mode hybridization and the SPP emission enhancement, we have varied the gap thickness from 1 nm to 10 nm. We have also varied the diameter D to keep the resonance wavelength fixed at $\lambda = 800$ nm. As shown in Fig. 6(a), for $H_d = 1$ nm, the SPP efficiency of the optimal geometry (red curve, $D = 39$ nm and $H = 72$ nm) is around 15%, which is 200 times bigger than the reference (blue curve, $D = 39$ nm and $H = 20$ nm). Moreover, as shown in Fig. S6(a), the SPP power emitted by the optimal antenna is 130 times larger than the reference. For $H_d = 2$ nm, as shown in Fig. 6(b), the SPP efficiency of the optimal geometry ($H = 90$ nm, $D = 74$ nm) is 50 times larger than the reference, while the SPP power is 30 times larger, see Fig. S6(b). Furthermore, as shown in Figs. 6(c)-(d), the SPP efficiency enhancement factor is smaller for larger gaps: 10 and 4 for $H_d = 5$ nm and $H_d = 10$ nm, respectively. In these two cases, the SPP power enhancement factors are 4 and 1.2, see Fig. S6(c)-(d). In summary, if the enhancement of SPP emission exists whatever the gap thickness, it is more pronounced for sub-5-nm gaps. For larger gaps, the gap mode S_{02} is less confined. Thus, the reference geometry performs better than for smaller gaps and using hybrid modes is less crucial.

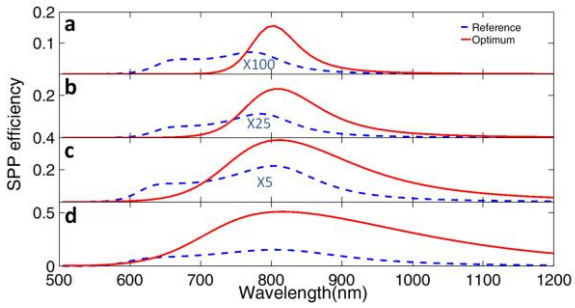

Figure 6. SPP efficiency spectrum for different values of the gap thickness, $H_d = 1$, 2, 5, and 10 nm. The nanopatch diameter is also varied ($D = 39$, 74, 147, and 220 nm) to keep the resonance wavelength fixed at $\lambda = 800$ nm. The optimal geometry (red curves) is compared to a reference geometry (blue dashed curves, $H = 20$ nm) that corresponds to the gap mode S_{02} decoupled from the antenna mode L_{01}. (a) $H_d = 1$ nm and $D = 39$ nm. The optimal geometry and the reference (spectrum multiplied by a factor of 100) correspond respectively to $H = 72$ nm and $H = 20$ nm. (b) $H_d = 2$ nm and $D = 74$ nm. The optimal geometry and the reference (spectrum multiplied by a factor of 25) correspond respectively to $H = 90$ nm and $H = 20$ nm. (c) $H_d = 5$ nm and $D = 147$ nm. The optimal geometry and the reference (spectrum multiplied by a factor of 5) correspond respectively to $H = 90$ nm and $H = 20$ nm. (d) $H_d = 10$ nm and $D = 220$ nm. The optimal geometry and the reference correspond respectively to $H = 90$ nm and $H = 20$ nm.

Increasing the SPP emission by tuning the surrounding refractive index

Let us finally explore the ratio between SPP emission and photon emission as well as the impact of the refractive index of the host medium on this ratio. We have computed the radiative efficiency P_r/P_T and the SPP efficiency of the optimal geometry (with hybrid modes) as a function of the refractive index of the host medium. The results are shown in Fig. 7; the radiative and SPP efficiencies are represented by circles and crosses, respectively. We have considered two cases: a nanopatch with $H_d = 1$ nm and $D = 39$ nm, and a nanopatch with $H_d = 1.5$ nm and $D = 56$ nm. The SPP and radiative efficiencies are computed at resonance, $\lambda = 800$ nm, see Fig. S7. For a nanopatch surrounded by air, the radiative and plasmonic efficiencies are almost equal. However, when the nanopatch is embedded in a medium with a larger refractive index, the SPP efficiency increases while the radiative efficiency decreases. For $H_d = 1.5$ nm,

the SPP efficiency is around 37% in a host medium with a refractive index of 2.8, whereas the corresponding radiative efficiency drops down to 5%. Hence, the refractive index is an efficient parameter to control the ratio between photon emission and SPP emission.

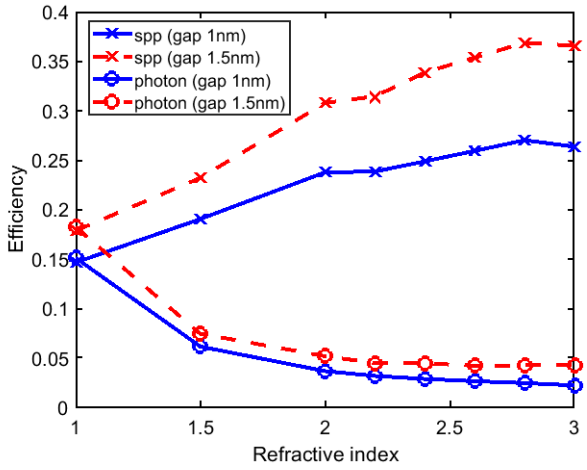

Figure 7. SPP efficiency (crosses) and radiative (photon emission) efficiency (circles) at resonance ($\lambda = 800$ nm) for the optimal geometries corresponding to ($H_d = 1$ nm, $D = 39$nm, blue solid curve) and ($H_d = 1.5$ nm and $D = 56$ nm, red dashed curve).

The decrease of the radiative efficiency can be easily understood. The radiative power P_r contains both the power radiated in air and the power radiated in the substrate. For a structure surrounded by air, the SPP is a leaky wave that radiates into the glass substrate and the power radiated in the substrate is dominated by the SPP leakage. Since the thickness of the gold film is 50 nm, the direct emission into the substrate is negligible. As the refractive index increases above 1.5, the SPP stops to leak into the glass substrate. Therefore, for $n > 1.5$, the radiative power contains only the power radiated in air. The latter being roughly constant, an increase of the refractive index results in the suppression of one radiative decay channel and thus a decrease of the radiative efficiency.

Conclusion

In summary, we have theoretically analyzed SPP emission in a cylindrical nanopatch antenna with a modal formalism. The nanopatch sustain two different families of modes,

the gap modes and the antenna modes. The first ones are strongly confined inside the dielectric gap and have an extremely large Purcell factor, $F_m \approx 10^6$. The downside of this tight confinement is a low efficiency to radiate SPPs, $\eta_{spp}^m \approx 1\%$. On the other hand, the field of antenna modes extends around the nanopatch, which results in a weaker confinement, a smaller Purcell factor ($F_m \approx 4 \times 10^4$), but a better SPP efficiency of 40% ($\eta_{spp}^m \approx 40\%$). For specific geometrical parameters, these two different modes couple. The coupling results in the appearance of two hybrid modes that retain the best properties of both worlds: a large Purcell factor ($F_m \approx 4 \times 10^5$) and a large modal SPP efficiency ($\eta_{spp}^m \approx 40\%$).

Using the hybridization mechanism allows increasing both the power emitted into SPPs and the SPP efficiency. For a gap of 1 nm, a diameter $D = 39$ nm, and a height $H = 72$ nm, over 2 orders of magnitude enhancement for the SPP power and a SPP efficiency of 15% can be obtained at $\lambda = 800$ nm. The power emitted into SPPs can be further enhanced by increasing the refractive index of the host medium. With a gap of 1 nm and a refractive index of 2.8, nearly 30% of SPP efficiency can be achieved. In a word, mode hybridization in a nanopatch antenna appears to be an important mechanism for engineering light-matter interactions in novel plasmonic platforms based on MIM nanogaps. Thanks to the efficiency improvement that is provides, this mechanism can open the way to the realization of efficient electrically driven plasmonic circuits. For extremely small gaps below 1 nm, non-local effects may be of importance.[49,50] In that case, the modal formalism and the two-modes approximation remain valid provided that the calculation of the eigenmodes takes non-locality into account.[51]

Competing Financial Interests

The authors declare no competing financial interest.

Acknowledgements

This work was supported by the French National Research Agency (ANR) under the project “Intelplan” (ANR-15-CE24-0020). C.Z. thanks the PhD scholarship supported

by the chair Safran-IOGS on Ultimate Photonics. JJ.G. thanks the support from Institut Universitaire de France.

Supporting Information

More details about (1) the gold permittivity used for the calculations, (2) the definition of the power emitted into surface plasmon polaritons, (3) quenching in a MIM nanopatch antenna, (4) quality factors and mode volumes, (5) validation of the modal formalism with only two modes, (6) dependence of the mode hybridization on the antenna geometry, and (7) dependence of the SPP emission on the refractive index of the surrounding medium.

References

(1) Purcell, E. M., *Phys. Rev.* **1946**, *69*, 681.

(2) Drexhage, K. H. Interaction of light with monomolecular dye layers. *Prog. Opt.* **1974**, *12*, 163-232.

(3) Barnes, W. Fluorescence near interfaces: the role of photonic mode density, *J. Mod. Opt.* **1998**, *45*, 661-699.

(4) Novotny, L.; Hecht, B. *Principles of nano-optics*, 2nd ed.; Cambridge University Press, 2012.

(5) Gérard, J.-M.; Sermage, B.; Gayral, B.; Legrand, B.; Costard, E.; Thierry-Mieg, V. Enhanced Spontaneous Emission by Quantum Boxes in a Monolithic Optical Microcavity. *Phys. Rev. Lett.* **1998**, *81*, 1110.

(6) Badolato, A.; Hennesy, K.; Atatüre, M.; Dreiser, J.; Hu, E.; Petroff, P. M.; Imamoglu, A. Deterministic Coupling of Single Quantum Dots to Single Nanocavity Modes" *Science* **2005**, *308*, 1158.

(7) Belacel, C.; Habert, B.; Bigourdan, F.; Marquier, F.; Hugonin, J.-P.; Michaelis de Vasconcellos, S.; Lafosse, X.; Coolen, L.; Schwob, C.; Javaux, C.; Dubertret, B.; Greffet, J.-J.; Senellart, P.; Maitre, A. Controlling spontaneous emission with plasmonic optical patch antennas. *Nano Lett.* **2013**, *13*, 1516.

(8) Santhosh, K.; Bitton, O.; Chuntonov, L.; Haran, G. Vacuum Rabi splitting in a plasmonic cavity at the single quantum emitter limit. *Nat. Commun.* **2016**, *7*, 11823.

(9) Chikkaraddy, R.; de Nijs, B.; Benz, F.; Barrow, S. J.; Scherman, O. A.; Rosta, E.; Demetriadou, A.; Fox, P.; Hess, O.; Baumberg, J. J. Single-molecule strong coupling at room temperature in plasmonic nanocavities. *Nature* **2016**, *535*, 127.

(10) Choy, J. T.; Hausmann, B. J. M.; Babinec, T. M.; Bulu, I.; Khan, M.; Maletinsky, P.; Yacoby, A.; Loncar, M. Enhanced single-photon emission from a diamond–silver aperture. *Nat. Photonics* **2011**, *5*, 738-743.

(11) Barik, A.; Chen, X.; Oh, S.-H. Ultralow-Power Electronic Trapping of Nanoparticles with Sub-10 nm Gold Nanogap Electrodes. *Nano Lett.* **2016**, *16*, 6317-6324.

(12) Roxworthy, B. J.; Ko, K. D.; Kumar, A.; Fung, K. H.; Chow, E. K. C.; Liu, G. L.; Fang, N. X.; Toussaint, K. C., Jr. Application of plasmonic bowtie nanoantenna arrays for optical trapping, stacking and sorting. *Nano Lett.* **2012**, *12*, 796−801.

(13) Kim, S.; Jin, J.; Kim, Y.-J.; Park, I.-Y.; Kim, Y.; Kim, S.-W. High-harmonic generation by resonant plasmon field enhancement. *Nature* **2008**, *453*, 757−760.

(14) Valentine, J.; Zhang, S.; Zentgraf, T.; Ulin-Avila, E.; Genov, D. A. Bartal, G.; Zhang, X. Three-dimensional optical metamaterial with a negative refractive index. *Nature* **2008**, *455*, 376−379..

(15) Moreau, A.; Ciraci, C.; Mock, J. J.; Hill, R. T.; Wang, Q.; Wiley, B. J.; Chilkoti, A.; Smith, D. R. Controlled-reflectance surfaces with film-coupled colloidal nanoantennas. *Nature*, **2012**, *492*, 86-90.

(16) Stewart, J. W.; Akselrod, G. M.; Smith, D. R.; Mikkelsen, M. H. Toward Multispectral Imaging with Colloidal Metasurface Pixels. *Adv. Mater.* **2017**, *29*, 1602971.

(17) Sakat, E.; Wojszvzyk, L.; Hugonin, J.-P.; Besbes, M.; Sauvan, C.; Greffet, J.-J. Enhancing thermal radiation with nanoantennas to create infrared sources with high modulation rates. *Optica*, **2018**, *5*, 175-179.

(18) Akselrod, G. M.; Argyropoulos, C.; Hoang, T. B.; Ciracì, C.; Fang, C.; Huang, J.; Smith, D. R.; Mikkelsen, M. H. Probing the mechanisms of large Purcell enhancement in plasmonic nanoantennas. *Nat. Photonics* **2014**, *8*, 835.

(19) Bidault, S.; Devilez, A.; Maillard, V.; Lermusiaux, L.; Guigner, J.-M.; Bonod, N.; Wenger, J. Picosecond Lifetimes with High Quantum Yields from Single-Photon-Emitting Colloidal Nanostructures at Room Temperature. *ACS Nano* **2016**, 4806-4815.

(20) Eggleston, M. S.; Messer, K.; Zhang, L.; Yablonovitch, E.; Wu, M. C. Optical antenna enhanced spontaneous emission. *PNAS* **2015**, *112*, 1704-1709.

(21) Jun, Y. C.; Pala, R.; Brongersma, M. L. Strong modification of quantum dot spontaneous emission via gap plasmon coupling in metal nanoslits. *J. Phys. Chem. C* **2010**, *114*, 7269-7273.

(22) Yuan, C. T.; Wang, Y. C.; Cheng, H. W.; Wang, H. S.; Kuo, M. Y.; Shih, M. H.; Tang, J. Modification of fluorescence properties in single colloidal quantum dots by coupling to plasmonic gap modes. *J. Phys. Chem. C* **2013**, *117*, 12762.

(23) Hoang, T. B.; Akselrod, G. M.; Argyropoulos, C.; Huang, J.; Smith, D. R.; Mikkelsen, M. H. Ultrafast spontaneous emission source using plasmonic nanoantennas. *Nat. Commun.* **2015**, *6*, 7788.

(24) Lambe, J.; McCarthy, S. L. Light Emission from Inelastic Electron Tunneling. *Phys. Rev. Lett.* **1976**, *37*, 923-925.

(25) Bigourdan, F.; Hugonin, J.-P.; Marquier, F.; Sauvan, C.; Greffet, J.-J. Nanoantenna for Electrical Generation of Surface Plasmon Polaritons. *Phys. Rev. Lett.* **2016**, *116*, 106803.

(26) Kern, J.; Kullock, R.; Prangsma, J.; Emmerling, M.; Kamp, M.; Hecht, B. Electrically driven optical antennas. *Nat. Photonics* **2015**, *9*, 582-586.

(27) Qian, H.; Hsu, S.-W.; Gurunatha, K.; Riley, C. T.; Zhao, J.; Lu, D.; Tao, A. R.; Liu, Z. Efficient light generation from enhanced inelastic electron tunnelling. *Nat. Photonics* **2018**, *12*, 485–488.

(28) Parzefall, M.; Szabó, Á.; Taniguchi, T.; Watanabe, K.; Luisier, M.; Novotny, L. Light from van der Waals quantum tunneling devices. *Nat. Commun.* **2019**, *10*, 292.

(29) Du, W.; Wang, T.; Chu, H.-S.; Nijhuis, C. A. Highly efficient on-chip direct electronic–plasmonic transducers. *Nat. Photonics*, **2017**, *11*, 623-627.

(30) Rose, A.; Hoang, T. B.; McGuire, F.; Mock, J. J.; Ciracì, C.; Smith, D. R.; Mikkelsen, M. H. Control

of radiative processes using tunable plasmonic nanopatch antennas. *Nano Lett.* **2014**, *14*, 4797.

(31) Faggiani, R.; Yang, J.; Lalanne, P. Quenching, Plasmonic, and Radiative Decays in Nanogap Emitting Devices. *ACS Photonics* **2015**, *2*, 1739-1744.

(32) Kongsuwan, N.; Demetriadou, A.; Chikkaraddy, R.; Benz, F.; Turek, V. A.; Keyser, U. F.; Baumberg, J. J.; Hess, O. Suppressed Quenching and Strong-Coupling of Purcell-Enhanced Single-Molecule Emission in Plasmonic Nanocavities. *ACS Photonics* **2018**, *5*, 186-191.

(33) Esteban, R.; Aguirregabiria, G.; Borisov, A. G.; Wang, Y. M.; Nordlander, P.; Bryant, G. W.; Aizpurua, J. The Morphology of Narrow Gaps Modifies the Plasmonic Response. *ACS Photonics* **2015**, *2*, 295-305.

(34) Tserkezis, C.; Esteban, R.; Sigle, D. O.; Mertens, J.; Herrmann, L. O.; Baumberg, J. J.; Aizpurua, J. Hybridization of plasmonic antenna and cavity modes: Extreme optics of nanoparticle-on-mirror nanogaps. *Phys. Rev. A* **2015**, *92*, 053811.

(35) Chikkaraddy, R.; Zheng, X.; Benz, F.; Brooks, L. J.; de Nijs, B.; Carnegie, C.; Kleemann, M.-E.; Mertens, J.; Bowman, R. W.; Vandenbosch, G. A. E.; Moshchalkov, V. V.; Baumberg, J. J. How Ultranarrow Gap Symmetries Control Plasmonic Nanocavity Modes: From Cubes to Spheres in the Nanoparticle-on-Mirror, *ACS Photonics* **2017**, *4*, 469-475.

(36) Huh, J.-H.; Lee, J.; Lee, S. Comparative Study of Plasmonic Resonances between the Roundest and Randomly Faceted Au Nanoparticles-on-Mirror Cavities. *ACS Photonics* **2018**, *5*, 413-421.

(37) Sauvan, C.; Hugonin, J. P.; Maksymov, I. S.; Lalanne, P. Theory of the spontaneous optical emission of nanosize photonic and plasmon resonators. *Phys. Rev. Lett.* **2013**, *110*, 237401.

(38) Lalanne, P.; Yan, W.; Vynck, K.; Sauvan, C.; Hugonin, J.-P. Light interaction with photonic and plasmonic resonances. *Laser Photonics Rev.* **2018**, *12*, 1700113.

(39) Weiss, T.; Muljarov, E. A. How to calculate the pole expansion of the optical scattering matrix from the resonant states. *Phys. Rev. B* **2018**, *98*, 085433.

(40) Colom, R.; McPhedran, R.; Stout, B.; Bonod, N. Modal expansion of the scattered field: causality, nondivergence and nonresonant contribution. *Phys. Rev. B* **2018**, *98*, 085418.

(41) Olmon, R. L.; Slovick, B.; Johnson, T. W.; Shelton, D.; Oh, S.-H.; Boreman, G. D.; Raschke, M. B. Optical dielectric function of gold. *Phys. Rev. B* **2012**, *86*, 235147.

(42) Hone, D.; Mühlschlegel, B.; Scalapino, D. J. Theory of light emission from small particle tunnel junction. *Appl. Phys. Lett.* **1978**, *33*, 203-204.

(43) Bigourdan, F.; Hugonin, J.-P.; Lalanne, P. Aperiodic-Fourier modal method for analysis of body-of-revolution photonic structures. *J. Opt. Soc. Am. A* **2014**, *31*, 1303-1311.

(44) Yang, J.; Hugonin, J.-P.; Lalanne, P. Near-to-far field transformations for radiative and guided waves. *ACS Photonics* **2016**, *3*, 395-402.

(45) Kurokawa, Y.; Miyasaki, H. T. Metal-insulator-metal plasmon nanocavities: Analysis of optical properties. *Phys. Rev. B* **2007**, *75*, 035411.

(46) Bozhevolnyi, S. I.; Sondergaard, T. General properties of slow-plasmon resonant nanostructures: nano-antennas and resonators. *Opt. Express* **2007**, *15*, 10869-10877.

(47) Yang, J.; Sauvan, C.; Jouanin, A.; Collin, S.; Pelouard, J.-L.; Lalanne, P. Ultrasmall metal-insulator-metal nanoresonators: impact of slow-wave effects on the quality factor. *Opt. Express* **2012**, *20*, 16880-16891.

(48) Yan, W.; Faggiani, R.; Lalanne, P. Rigorous modal analysis of plasmonic nanoresonators. *Phys. Rev. B* **2018**, *97*, 205402.

(49) Ciraci, C.; Hill, R. T.; Mock, J. J.; Urzhumov, Y.; Fernandez-Dominguez, A. I.; Maier, S. A.; Pendry,

J. B.; Chilkoti, A.; Smith, D. R. Probing the ultimate limits of plasmonic enhancement. *Science* **2012**, *337*, 1072-1074.

(50) Moreau, A.; Ciraci, C.; Smith, D. R. Impact of nonlocal response on metallodielectric multilayers and optical patch antennas. *Phys. Rev. B* **2013**, *87*, 045401.

(51) Dezfouli, M. K.; Tserkezis, C.; Mortensen, N. A.; Hughes, S. Nonlocal quasinormal modes for arbitrarily shaped three-dimensional plasmonic resonators. *Optica* **2017**, *4*, 1503-1509.

Supporting information for

Surface plasmon polaritons emission with nanopatch antennas: enhancement by means of mode hybridization

Cheng Zhang, Jean-Paul Hugonin, Jean-Jacques Greffet and Christophe Sauvan*

Laboratoire Charles Fabry, Institut d'Optique Graduate School, CNRS, Université Paris-Saclay, 91127 Palaiseau, France
**Corresponding author: christophe.sauvan@institutoptique.fr*

Content

1. Gold permittivity used for the calculations

The dielectric permittivity of gold that we have used for the calculations is given by a Drude-Lorentz model that fits the data tabulated in [1] over the [500-1500] nm spectral range,

$$\varepsilon_m(\omega) = \varepsilon_\infty - \frac{\omega_p^2}{\omega^2 + i\omega\gamma_D} - \frac{A_L}{\omega^2 - \omega_L^2 + i\omega\gamma_L} \ , \qquad \text{(S1)}$$

with $\omega = 2\pi c/\lambda$ the angular frequency, $\varepsilon_\infty = 6$, $\omega_p = 1.317 \times 10^{16}$ rad.s^{-1} the plasma frequency, $\gamma_D = 6.216 \times 10^{13}$ rad.s^{-1} the damping of the free electrons gas, $\omega_L = 4.572 \times 10^{15}$ rad.s^{-1} the resonance frequency of the oscillator used in the Lorentz model, $\gamma_L = 1.332 \times 10^{15}$ rad.s^{-1} the oscillator damping, and $A_L = 1.5\omega_L^2$ the oscillator strength.

2. Definition of the power emitted into surface plasmon polaritons

Since we consider a real metal with a finite conductivity, the modes are not orthogonal in the sense of the Poynting vector, as is usually the case in lossless waveguides. In such an absorbing system, the modes obey the general unconjugated form of orthogonality.[2] Therefore, the total power (total Poynting vector) carried out by several excited modes cannot be expressed as a sum over the Poynting vectors of each mode; interference terms between the different modes appear in the expression of the total power. In the context of surface plasmon polariton (SPP) propagation along metal surfaces, these interferences have a non-negligible impact, as experimentally demonstrated in [3].

The main practical consequence is that the concept of power carried out by a SPP is less meaningful than in a usual lossless waveguide. However, it is still possible to define the power carried out by SPPs as the Poynting vector associated to the fraction of the total field corresponding to SPPs [first term in Eq. (1), main text]. This modal Poynting vector, integrated over the azimuthal angle θ, is proportional to $\frac{4}{|k_{spp}|}\left|A_{spp}\right|^2 \exp\left[-2\mathrm{Im}\left(k_{spp}\right)r\right]$, where the exponentially-decreasing factor corresponds to the SPP attenuation along the interface. Thus, the quantity $\frac{4}{|k_{spp}|}\left|A_{spp}\right|^2$ is a meaningful figure of merit for quantifying the amount of SPP propagating along the metal surface. We define the power emitted into SPPs as

$$P_{spp} = \frac{4}{|k_{spp}|}\left|A_{spp}\right|^2. \tag{S2}$$

3. Quenching in a MIM nanopatch antenna

The power P_q defined in Eq. (6) in the main text, which is associated to the excitation of higher-order modes, corresponds to quenching, as demonstrated in [4]. To avoid the cumbersome calculation of hundreds of higher-order quasinormal modes, we assume that the quenching in a nanopatch antenna is the same as the quenching in the associated metal-insulator-metal (MIM) planar system. This assumption is valid provided that the radial size of the nanopatch is larger than a few nanometers, the typical size where the absorption associated to quenching takes place. The quenching in the planar system is calculated according to the procedure proposed in [5], i.e., by making the difference between the total power emitted in the planar system and the power emitted in the gap SPP. Note that, since the gold thicknesses H and H_m are larger than the skin depth, considering the real air/gold/dielectric/gold/dielectric stack or a simplified gold/dielectric/gold stack provides the same result for the calculation of P_q.

Figure S1 displays the value of the quenching P_q in a planar MIM system as a function of the wavelength and the gap thickness between 1 and 10 nm. The quenching increases as the wavelength or the gap thickness is decreased. For instance, for $\lambda = 800$ nm and a gap thickness $1 < H_d < 2$ nm, $P_q \approx 10^5 P_0$. Therefore, using a nanoantenna allows overcoming quenching if, and only if, this nanoantenna supports a mode with a Purcell factor of the order of 10^5.

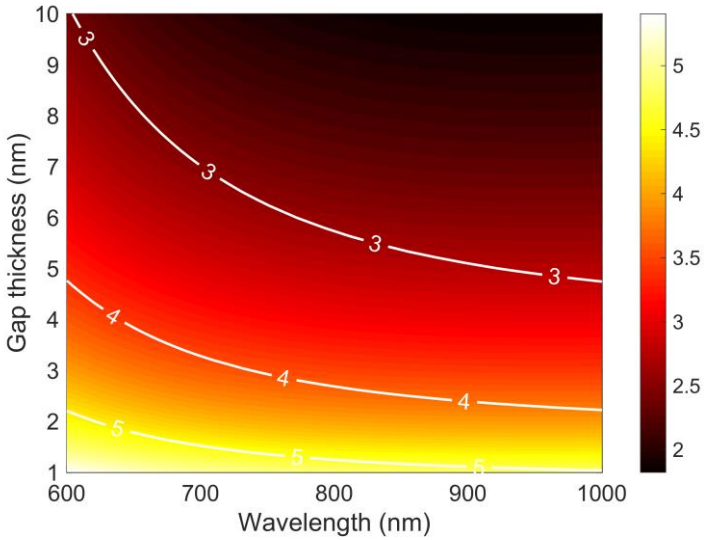

Figure S1. Quenching P_q (log scale) in a planar gold – dielectric $n_d = 1.45$ – gold stack as a function of the wavelength and the gap thickness. The dipole source is located at half-distance from both metal surfaces. The power P_q is normalized by the power P_0 emitted by the same dipole in a bulk medium of refractive index $n_d = 1.45$. The three white curves show the wavelength and thickness values for which $P_q = 10^5 P_0$, $10^4 P_0$, and $10^3 P_0$, respectively.

4. Quality factors and mode volumes

We provide here the quality factors and the volumes of the modes considered in Fig. 3 in the main text. The quality factors of the S_{02}, L_{01}, and S_{11} modes are shown in Fig. S2 as a function of the nanopatch height. The antenna mode L_{01} has a lower quality factor, $Q \approx 10$, than the gap modes S_{02} and S_{11}, $Q \approx 25$.

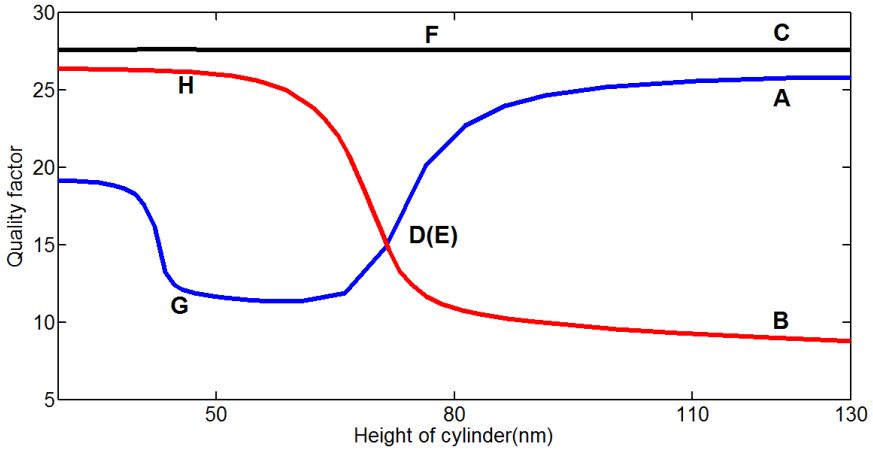

Figure S2. Quality factors as the function of the nanopatch height. The marks A, B, C, D, E, F, G, and H correspond to those in Fig. 3 in the main text. A, B, and C mark respectively the uncoupled gap mode S_{02}, the uncoupled antenna mode L_{01}, and the gap mode S_{11}. The marks D and E correspond to the hybrid modes resulting from the coupling between modes S_{02} and L_{01}. Note that the increase of the quality factor of the blue curve for small heights (on the left of point G) is due to the coupling of the antenna mode L_{01} with a higher-order gap mode with an azimuthal number $m = 0$. This coupling is not shown in Fig. 3 in the main text.

For a nanopatch height $H = 120$ nm, the volume of the antenna mode L_{01} is $(6.7 + 0.9i)/10^5(\lambda/n_d)^3$ while that of the gap mode S_{02} is one order of magnitude smaller, $(7.1 - 0.3i)/10^6(\lambda/n_d)^3$. For a smaller height $H = 52$ nm, the L_{01} mode is slightly less confined with $V = (3.5 + 1.2i)/10^4(\lambda/n_d)^3$ and the S_{02} gap mode is still extremely small, $V = (6.8 + 0.4i)/10^6(\lambda/n_d)^3$. For a nanopatch height of 72 nm that corresponds to the maximum coupling between the modes, the quality factor of the antenna mode is slightly raised up to 15 (see Fig. S2) while the mode volume is reduced to $(9.3 - 6.7i)/10^6(\lambda/n_d)^3$, a value comparable to the volume of the uncoupled gap mode.

5. Validation of the modal formalism with only two modes

Figure S3 shows a comparison between the predictions of the modal formalism with two modes and the results of a rigorous calculation of the full electromagnetic field with the aperiodic Fourier modal method (a-FMM) for body-of-revolution structures.[6] The excellent agreement observed for $\lambda > 750$ nm in Fig. S3(a) (total power) validates the assumption that the quenching P_q is the same in the nanopatch and in the planar MIM system. The good agreement observed for the SPP power in Fig. S3(b) validates the assumption that higher-order modes of the nanoantenna do not contribute to the generation of propagating SPPs, see Eq. (12) in the main text.

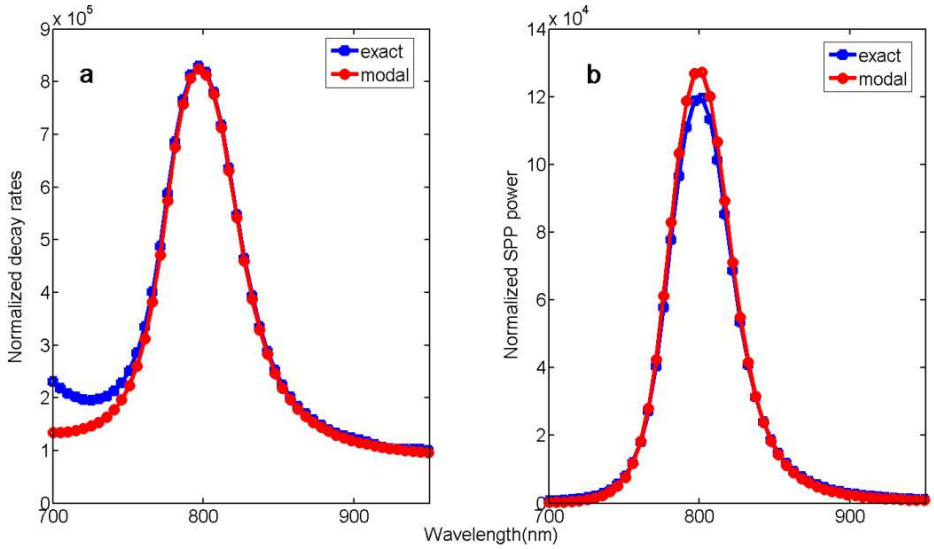

Figure S3. Comparison between the bimode formalism and exact numerical calculations with an antenna height of $H = 72$ nm, a diameter $D = 39$ nm, and a gap thickness $H_d = 1$ nm. (a) Total power P_T. The predictions of the modal formalism [red dots line, see Eq. (6) in the main text] are in excellent agreement with rigorous calculations of the full Green tensor (blue dots line). The discrepancy for $\lambda < 750$ nm is due to (i) the excitation of a higher-order gap mode that is not considered and (ii) the failure of the assumption that the quenching in the nanopatch is the same as in the planar MIM system. (b) SPP power P_{spp}. The predictions of the modal formalism [red dots line, see Eq. (12) in the main text] are in good agreement with exact calculations (blue dots line). Both P_T and P_{spp} have been normalized by the emission of the same dipole in a bulk medium of refractive index n_d.

6. Dependence of the mode hybridization on the antenna geometry

Figures S4 and S5 provide additional data on the modification of the coupling between the antenna mode L_{01} and the gap mode S_{02} as the nanopatch diameter is varied with a fixed gap thickness $H_d = 1.5$ nm. The variation with the cylinder height of the resonant wavelengths corresponding to the antenna mode L_{01} and the gap mode S_{02} is shown in Fig. S4 for different values of the nanopatch diameter. Figure S5 displays the variation of the quality factors. By choosing a diameter of 25 nm, 40 nm, 56 nm, and 90 nm, the gap mode S_{02} is tuned to 615 nm, 710 nm, 790 nm, and 970 nm. Varying the antenna height leads to an anti-crossing of the resonance frequencies in the first three cases and to a crossing in the case of the largest diameter. A splitting of 33 meV, 51 meV, and 25 meV is obtained from (a) to (c). Because the coupling strength depends on the cavity loss and the mode volume, it is interesting to point out that a lower quality factor of the gap mode S_{02} and a larger mode volume (corresponding to a larger diameter) lead to a smaller coupling strength.

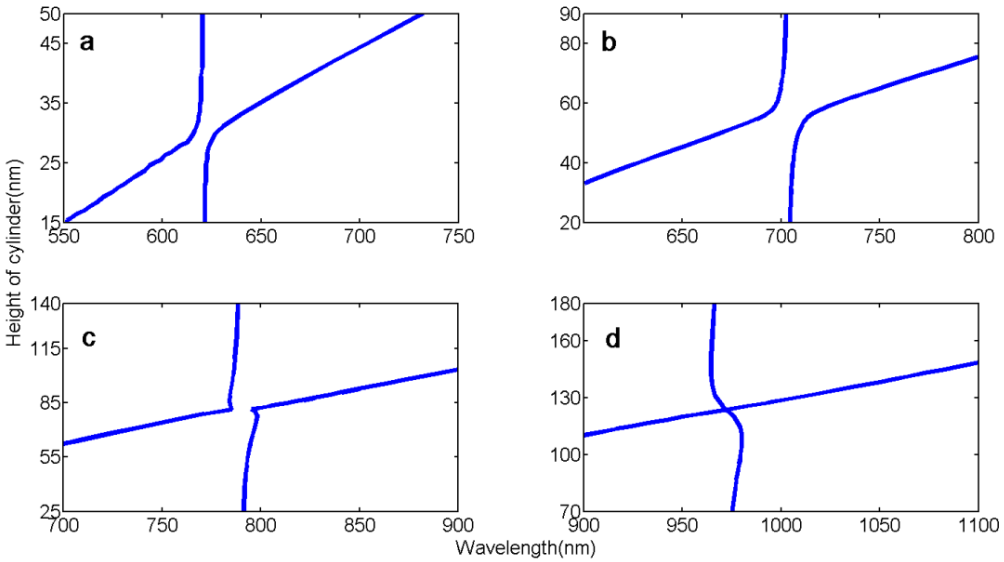

Figure S4. Impact of the nanopatch diameter on the coupling between the antenna mode L_{01} and the gap mode S_{02}. The real part of the eigenfrequencies are represented as a function of the cylinder height. Each figure corresponds to a different cylinder diameter of 25 nm (a), 40 nm (b), 56 nm (c) and 90 nm (d).

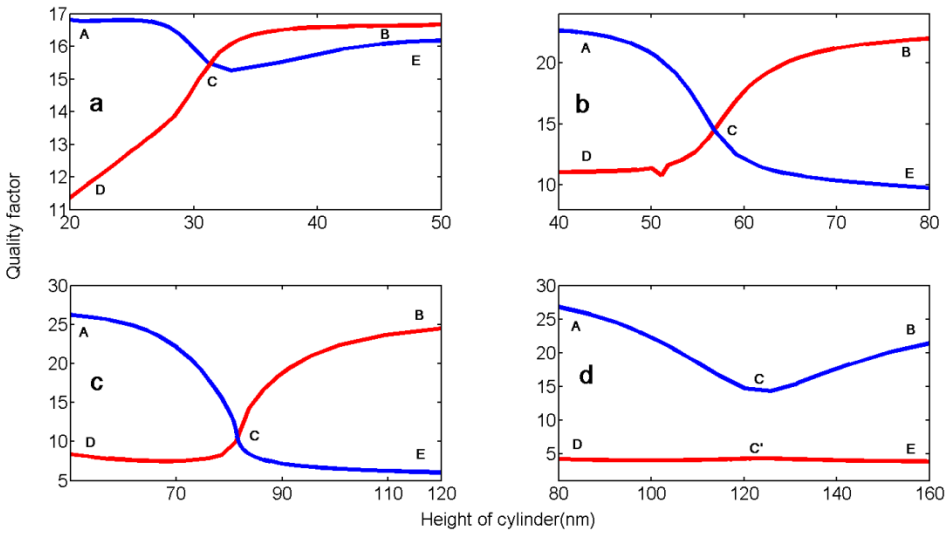

Figure S5. Quality factors of the L_{01} and S_{02} modes as a function of the naopatch height with a fixed gap thickness of 1.5 nm. Each figure corresponds to a different cylinder diameter of 25 nm (a), 40 nm (b), 56 nm (c) and 90 nm (d). (a-c) The curves A-C-B D-C-E show the evolution of the S_{02} mode and the L_{01} mode, respectively. (d) The curve A-C-B corresponds to the S_{02} mode and the curve D-C'-E corresponds to the L_{01} mode.

Figure S6 show the SPP power spectra of the optimal geometry for different values of the gap thickness, $H_d = 1$ nm, $H_d = 2$ nm, $H_d = 5$ nm, and $H_d = 10$ nm.

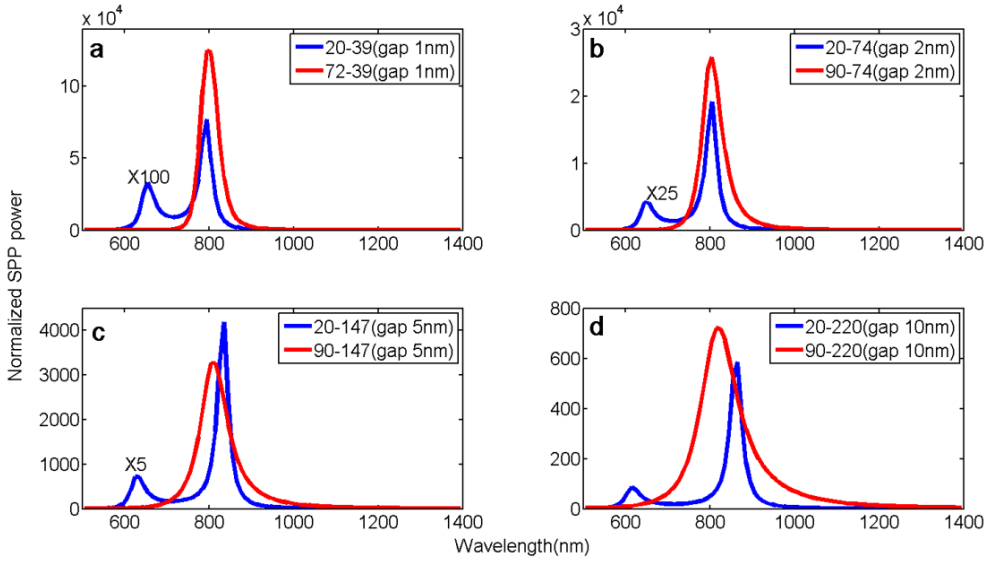

Figure S6. Normalized SPP power spectra (red curves) of the optimal structures that resonates at 800 nm for different values of the gap thickness, 1 nm, 2 nm, 5 nm, and 10 nm, respectively. The optimal antennas are compared to a reference ($H = 20$ nm, blue curves) that corresponds a geometry for which the gap mode S_{02} is decoupled from the antenna mode L_{01}. The values of the different geometrical parameters are the same as in Fig. 5 in the main text.

7. Increasing the SPP emission by tuning the surrounding refractive index

We provide here additional data on the increase of the SPP emission as the refractive index of the host medium is increased. Fig. S7 shows the total power, the SPP power and the radiative power as a function of the wavelength for different values of the refractive index of the host medium. The purpose of this graph is to illustrate the spectral changes in the emission due to the modification of the refractive index. As the refractive index increases, the spectrum redshifts. The SPP power increases whereas the radiative power decreases. On the other hand, the total power slightly decreases. This results in the increase of the SPP efficiency and the decrease of the radiative efficiency shown in Fig. 6 in the main text. Fig. S8 shows the nonradiative efficiency of the antenna, i.e., the ratio of the total power that is dissipated in the metal.

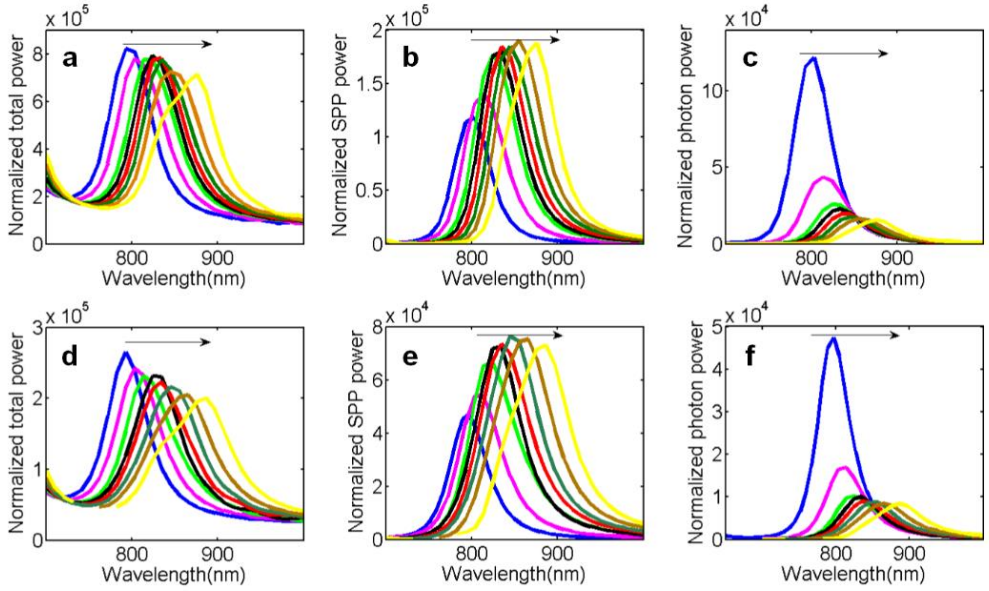

Figure S7. Total power spectra, SPP power spectra, and radiative power spectra for increasing values of the refractive index of the host medium (from 1 to 3, the increment direction follows the arrow direction). (a-c) For a gap thickness of 1 nm and a nanopatch diameter of 39 nm. (d-f) For a gap thickness of 1.5 nm and a nanopatch diameter of 56 nm. Each curve is plotted for the optimal antenna height, i.e., at the optimal coupling between the gap mode S_{02} and the antenna mode L_{01}.

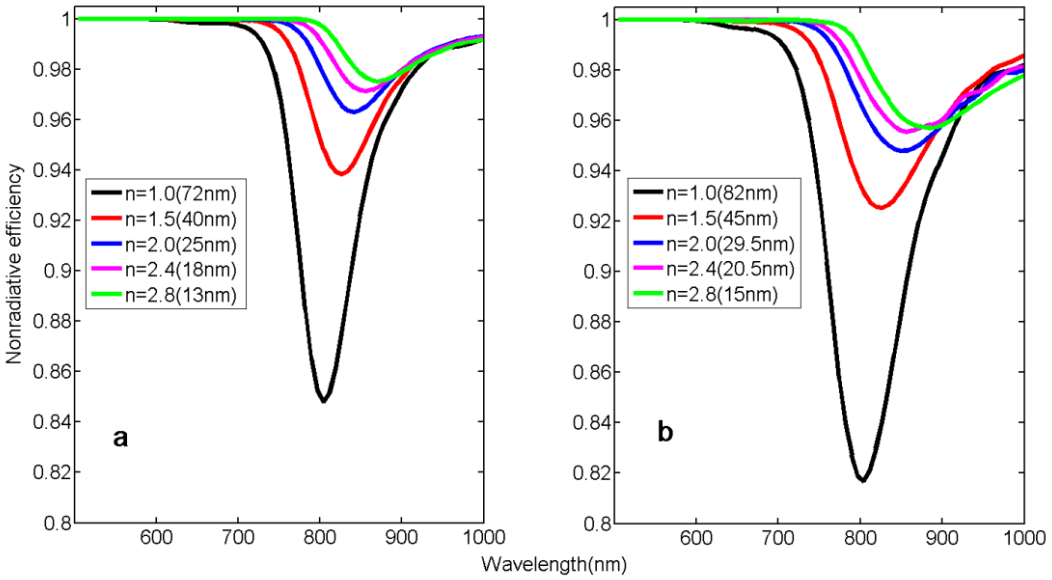

Figure S8. Nonradiative efficiency spectra for different values of the refractive index of the host medium from 1 to 2.8. (a) Spectra of the optimal structures for a gap thickness of 1 nm and an antenna diameter of 39 nm; (b) Spectra of the optimal structures for a gap thickness of 1.5 nm and an antenna diameter of 56 nm.

8. References

(1) Olmon, R. L.; Slovick, B.; Johnson, T. W.; Shelton, D.; Oh, S.-H.; Boreman, G. D.; Raschke, M. B. *Optical dielectric function of gold. Phys. Rev. B* **2012**, *86*, 235147.

(2) Snyder, A. W.; Love, J. *Optical waveguide theory*; Springer Science & Business Media, 2012.

(3) Lozan, O.; Perrin, M.; Ea-Kim, B.; Rampnoux, J. M.; Dilhaire, S.; Lalanne, P. *Anomalous Light Absorption around Subwavelength Apertures in Metal Films. Phys. Rev. Lett.* **2014**, *112*, 193903.

(4) Yan, W.; Faggiani, R.; Lalanne, P. *Rigorous modal analysis of plasmonic nanoresonators. Phys. Rev. B* **2018**, *97*, 205422.

(5) Faggiani, R. m.; Yang, J.; Lalanne, P. *Quenching, plasmonic, and radiative decays in nanogap emitting devices. ACS Photonics* **2015**, *2*, 1739.

(6) Bigourdan, F.; Hugonin, J.-P.; Lalanne, P. *Aperiodic-Fourier modal method for analysis of body-of-revolution photonic structures. JOSA A* **2014**, *31*, 1303.